J Neurophysiol 103: 3501–3515, 2010.
First published April 14, 2010; doi:10.1152/jn.00155.2010.

NMDAR-Dependent Control of Call Duration in *Xenopus laevis*

Erik Zornik, Abraham W. Katzen, Heather J. Rhodes, and Ayako Yamaguchi
Biology Department, Boston University, Boston, Massachusetts

Submitted 4 February 2010; accepted in final form 10 April 2010

Zornik E, Katzen AW, Rhodes HJ, Yamaguchi A. NMDAR-dependent control of call duration in *Xenopus laevis*. *J Neurophysiol* 103: 3501–3515, 2010. First published April 14, 2010; doi:10.1152/jn.00155.2010. Many rhythmic behaviors, such as locomotion and vocalization, involve temporally dynamic patterns. How does the brain generate temporal complexity? Here, we use the vocal central pattern generator (CPG) of *Xenopus laevis* to address this question. Isolated brains can elicit fictive vocalizations, allowing us to study the CPG in vitro. The *X. laevis* advertisement call is temporally modulated; calls consist of rhythmic click trills that alternate between fast (~60 Hz) and slow (~30 Hz) rates. We investigated the role of two CPG nuclei—the laryngeal motor nucleus (n.IX–X) and the dorsal tegmental area of the medulla (DTAM)—in setting rhythm frequency and call durations. We discovered a local field potential wave in DTAM that coincides with fictive fast trills and phasic activity that coincides with fictive clicks. After disrupting n.IX–X connections, the wave persists, whereas phasic activity disappears. Wave duration was temperature dependent and correlated with fictive fast trills. This correlation persisted when wave duration was modified by temperature manipulations. Selectively cooling DTAM, but not n.IX–X, lengthened fictive call and fast trill durations, whereas cooling either nucleus decelerated the fictive click rate. The *N*-methyl-D-aspartate receptor (NMDAR) antagonist DAPV blocked waves and fictive fast trills, suggesting that the wave controls fast trill activation and, consequently, call duration. We conclude that two functionally distinct CPG circuits exist: *1*) a pattern generator in DTAM that determines call duration and *2*) a rhythm generator (spanning DTAM and n.IX–X) that determines click rates. The newly identified DTAM pattern generator provides an excellent model for understanding NDMAR-dependent rhythmic circuits.

INTRODUCTION

Many rhythmic motor behaviors consist of multiple simple rhythms woven into temporally and/or spatially intricate patterns. We sought to understand the neural mechanisms by which discrete rhythms are temporally organized. A major obstacle to understanding temporal patterning lies in the complexity of many behaviors. For example, the control of behaviors such as birdsong or vertebrate locomotion involves the coordination of many muscle groups in elaborate patterns of activation.

In this study, we investigated the neural basis of temporal patterning of calling in the frog, *Xenopus laevis*. *Xenopus* vocalizations are generated by a simple mechanism of sound production. Calls are produced independent of respiratory movements (unlike most other vertebrate vocal mechanisms) by a single pair of laryngeal muscles. Despite this mechanistic simplicity, the most common male vocalization—advertisement call—is temporally complex, allowing us to explore how a tractable neuronal circuit generates elaborate temporal patterns.

Address for reprint requests and other correspondence: E. Zornik, Boston University, Biology Department, Boston, MA 02215 (E-mail: ez@bu.edu).

Each advertisement call consists of two click trills, fast (~60 Hz) followed by slow (~30 Hz), occasionally preceded by an introductory phase (~20–40 Hz; Fig. 1; Tobias et al. 1998, 2004; Yamaguchi et al. 2008). Fast and slow trills last close to 200 and 800 ms, respectively, and introductory phases are variable in duration. Previously, we demonstrated that advertisement calls are generated by a central pattern generator (CPG; Rhodes et al. 2007). The vocal CPG functions on two distinct timescales. On a shorter (millisecond) timescale, the CPG produces distinct rhythms (in Hertz): roughly 60, 30, and 20–40 Hz. On a longer timescale, the CPG controls the temporal pattern of trill delivery, with each trill lasting hundreds of milliseconds and calls repeating about once/s.

The *Xenopus* vocal CPG can be readily studied in vitro. A compound action potential (CAP) on the motor nerve precedes each click produced by the larynx (Yamaguchi and Kelley 2000); thus nerve activity provides a direct readout of behavior. An isolated brain preparation generates fictive vocalizations (with bath-applied serotonin [5-HT]) that are similar to in vivo advertisement calls (Rhodes et al. 2007). The vocal CPG contains two reciprocally connected nuclei: the laryngeal motor nucleus (n.IX–X) and the dorsal tegmental area of medulla (DTAM; Brahic and Kelley 2003, Kelley 1980; Wetzel et al. 1985), which is also called pretrigeminal nucleus by Schmidt (1992). In this study, we examined the roles played by the two CPG nuclei in regulating rhythms (shorter timescale) and patterns (longer timescale).

We discovered a local field potential (LFP) wave endogenous to DTAM that coincided with fictive fast trills; this activity resembled slow-wave activity originally identified in the DTAM homologue of the leopard frog (Schmidt 1992). We used temperature and *N*-methyl-D-aspartate receptor (NMDAR) perturbations to investigate the involvement of this LFP wave in determining the temporal structure of motor output. Furthermore, we discovered phasic activity in DTAM LFP that correlates with fictive clicks and requires intact connections between DTAM and n.IX–X. Our findings indicate that the vocal CPG includes two functionally distinct, though anatomically overlapping, neural circuits. One circuit, including neurons in DTAM and n.IX–X (with required connections between the two nuclei), functions as a rhythm generator that determines the click rates of fast and slow trills. The second circuit, a pattern generator, is endogenous to DTAM and produces the NMDAR-dependent slow wave, which in turn acts on the rhythm generator to determine the timing of fast trill onset and offset.

METHODS

Animals

We obtained adult male *Xenopus laevis* from Nasco (Fort Atkinson, WI). Ten animals (weight, 56.3 ± 13.6 g; length, 7.5 ± 0.8 cm) were

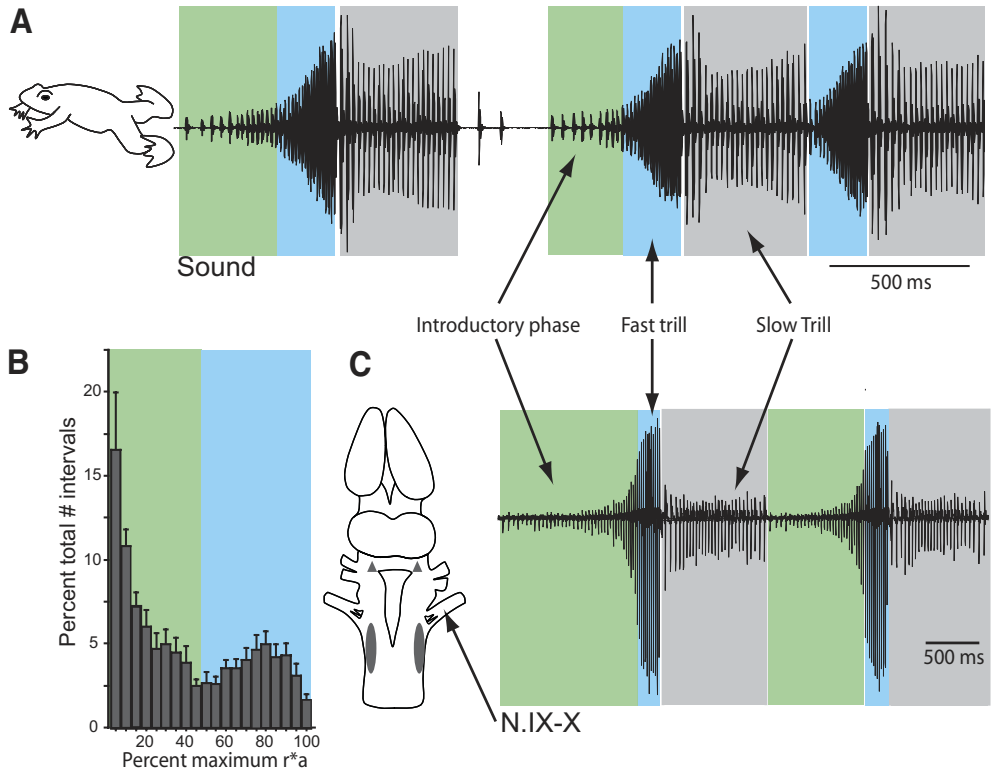

FIG. 1. Defining vocal trills: introductory phase, fast trill, and slow trill. *A*: recordings from intact frogs; sound oscillogram of 3 male advertisement calls from the beginning of a calling episode. The first 2 calls contain a longer introductory phase, consisting of low-amplitude, slow-rate clicks (green boxes). The third and subsequent (not shown) calls are lacking the introductory phases. The blue and gray boxes overlying the call delineates the duration of the fast and slow trills, respectively. In vivo, introductory phases occur only at the beginning of calling episodes (e.g., one or two initial calls in a series of calls) and the remaining calls consist of only fast and slow trills as in the last call shown. *B*: frequency histogram of fictive compound action potential (CAP) interval data. The products of instantaneous rate and amplitude (r*a) were calculated for fictive fast trill intervals (all CAPs except slow trill CAPs), normalized to the maximum value, and divided into 5% bins. Bins were then averaged across 11 animals and plotted in the final histogram shown (mean ± SE). The histogram shows a peak around 80%, representing fictive fast trill intervals, with the rest skewed toward zero (introductory intervals). Fictive fast trill onset was defined as the first interval in which the product of r*a exceeds 50% maximum r*a (blue). Intervals below that point are defined as fictive introductory phase intervals (green; see METHODS). *C*, *left*: diagram of a dorsal view of the *X. laevis* brain (dorsal tegmental area of the medulla [DTAM] is represented by triangles, ovals denote laryngeal motor nucleus (n.IX–X), and arrow points to the laryngeal nerve, N.IX–X). *Right*: nerve recording of 2 fictive advertisement calls showing the resulting designation of introductory phase (green), fast trill (blue), and slow trill (gray). The same color scheme is used to highlight each trill type in subsequent figures.

used for in vivo vocal recording experiments; 61 frogs (weight, 39.1 ± 5.9 g; length, 6.7 ± 0.4 cm) were used for in vitro experiments. Animals were kept in glass aquaria and maintained on a 12-h:12-h light:dark cycle. All procedures were approved by the Institutional Animal Care and Use Committee at Boston University and complied with National Institutes of Health guidelines.

Vocal recordings

A previous study showed that in vivo click and in vitro CAP rates are dependent on temperature (Yamaguchi et al. 2008). Here, we extended our previous study by examining how temperature affected call and trill durations in vivo. The results of this experiment allowed us to quantitatively characterize the thermal sensitivity of vocal rhythms and patterns in vivo and to compare it to data obtained in vitro (described in the following text). Ten adult males were administered human chorionic gonadotropin (hCG; 600–1,000 IU; Sigma, St. Louis, MO) injected subcutaneously to elicit advertisement calling (Wetzel and Kelley 1983; Yamaguchi et al. 2008). Animals were placed in a 38 L aquarium; vocalizations were recorded with a hydrophone (H2; Aquarium Audio Products, Anacortes, WA) and a sound-activated recording system (Syrinx software, www.syrinxpc.com; John Burt). Each male was recorded at two temperatures, 18 and 26°C. Tank warming was achieved with an aquarium heater (VISI Therm type VTH 1000 heater; Aquarium Systems, Mentor, OH) and the cool temperature was maintained by setting the room temperature to 18°C. Tank temperature was measured using a Traceable digital thermometer (−58°F ± 158°F; Fisher Scientific, Waltham, MA). Males were paired in the tank with a female, which is known to stimulate advertisement calling (Tobias et al. 1998; Wetzel et al. 1983).

Isolated brain preparation and fictive vocal recordings

Fictive vocalizations could be effectively elicited from sexually mature adult males without prior injection of hCG. To isolate brains for fictive vocal recordings, animals were injected subcutaneously with 500 μl 1.3% tricaine methanesulfonate (MS-222; Sigma). Once anesthetized, animals were placed on ice and decapitated. Skulls were placed in a dish containing ice-cold saline (in mM: 96 NaCl, 20 $NaHCO_3$, 2 $CaCl_2$, 2 KCl, 0.5 $MgCl_2$, 10 HEPES, and 11 glucose, pH 7.8), oxygenated with 99% O_2, and brains were promptly removed. After removal, and between recordings, brains were pinned to a silicone elastomer-lined (Sylgard; Dow Corning, Midland, MI) petri dish (150 mm diameter) containing oxygenated saline (~200 ml). For recordings, brains were transferred to a recording chamber (Sylgard-lined 50 mm diameter petri dish: 20 ml volume).

Laryngeal nerve activity was recorded using a suction electrode placed over cranial nerve (N.) IX–X, with all roots cut except the most caudal (containing all laryngeal motor neuron axons; Simpson et al. 1986). For LFP recordings in DTAM, the pia covering the cerebellum (lying dorsal to DTAM) was removed and a 1 MΩ tungsten electrode

(FHC, Bowdoin, ME) was placed in DTAM (~100 μm posterior to the tectum–cerebellum border, ~200 μm from the lateral edge of the fourth ventricle and 650 μm below the pial surface). In some experiments, LFP recordings in DTAM were obtained from transected brains in which connections with n.IX–X were severed. In these preparations, iridectomy scissors were used to transect the brain at the caudal edge of N.VIII and brains were allowed to recover at least 1 h.

Fictive vocalizations and DTAM waves were elicited by bath-application of 5-HT (Sigma). Superfusion of saline through the recording chamber was suspended and 1 ml of concentrated 5-HT solution (0.6 mM in saline) was added to the 20 ml bath (30 μM, final concentration). Nerve and LFP signals were amplified ×1,000 using differential amplifiers (Models 1700 and 1800, respectively; A-M Systems, Carlsborg, WA) and band-pass filtered (10 Hz to 5 kHz and 0.1–5 kHz, respectively). All signals were digitized at 10 kHz (Digidata 1322A; Molecular Devices, Sunnyvale, CA) and recorded on a PC using Clampex software (Molecular Devices). After nearly 5 min of recording, superfusion was reinstated at the maximum rate (~10 ml/min) for 5 min to wash out the 5-HT, after which brains were then returned to the larger holding dish. Brains were incubated in oxygenated saline for 1 h between all 5-HT applications.

Whole-bath and local temperature manipulations

Although the DTAM wave appeared to correlate with onset and offset of trills, the stereotyped nature of call and trill durations precluded quantitative analysis of the association between the two events. However, temperature manipulation provides a means by which to assess this correlation over a broad range of wave durations. To determine the effect of brain temperature on waves and fictive vocalizations, we clamped the temperature of the recording bath at three or four distinct temperatures (range, 15.6–23.6°C). This was achieved by superfusing the recording chamber with warm (~26°C) or cool (~16°C) saline with 30 μM 5-HT as needed. Bath temperature was monitored using a thermocouple microprobe (IT-24P, 250 μm OC; Physitemp, Clifton, NJ) connected to a digital thermometer (BAT-12, 0.1° resolution; Physitemp), and recorded using the Digidata/Clampex setup.

To determine the effect of selectively cooling either DTAM or n.IX–X on the fictive vocalizations (specifically rhythms and patterns), we developed a new technique in this study. In a previous study, we selectively cooled DTAM by inserting a cryoprobe directly into the nucleus (Yamaguchi et al. 2008). Unfortunately, mere placement of this probe into n.IX–X (at bath temperature) eliminated calling, thus preventing us from selectively cooling n.IX–X using the same method (for comparison with DTAM effects). This outcome led us to conclude that n.IX–X is highly sensitive to mechanical disturbances. To circumvent this, we developed a new selective cooling method involving a split-bath technique. For selective cooling of brain regions containing DTAM or n.IX–X, we made a bisected recording chamber separated across its diameter by a thin plastic wall (inserted into the Sylgard lining) interrupted in the center by a 4 mm space just large enough to contain the width of the brain. The brain was pinned so that the wall bisected the rostral and caudal part of the hindbrain at the caudal edge of N.VIII. A free plastic piece (with a cutout to fit the brain) was attached to the main plastic wall (a thin coating of petroleum jelly ensured a good seal), thus closing the 4 mm gap and separating the two portions of the brain. In this configuration, DTAM and n.IX–X were in separate chambers, each about 1.5 mm from the dividing wall. Thermocouple probes were placed next to n.IX–X and DTAM (one of each bilateral pair) to monitor the local temperature on each side of the divider. To maintain distinct local temperatures, we removed the saline and applied low-concentration agarose (0.3% made in oxygenated saline). Chilled agarose was then added to one chamber to selectively cool one side (~18°C) while keeping the other side warm (~22°C), adding warm agarose if necessary. To elicit fictive vocalizations, 10 μl of 0.6 mM 5-HT was applied over the agarose. Additional cool or warm agarose was added to the appropriate chamber to maintain the desired temperature difference during fictive vocal recordings. Because vocal nuclei anterior to DTAM are not required for vocal production (Yu and Yamaguchi 2010), we refer to cooling the anterior chamber as "selective DTAM cooling" because this is the only CPG component being cooled. Likewise, cooling of the posterior chamber is referred to as "selective n.IX–X cooling" because n.IX–X is the sole CPG nucleus in this part of the brain. Selective DTAM and n.IX–X cooling were performed in random order, followed by a 22°C control in both chambers. Data were collected after the intended temperature gradient was established for ≥30 s. Data were used only if all three treatments (DTAM cooling, n.IX–X cooling, and control) yielded at least five fictive advertisement calls.

APV application

To determine the role of NMDARs in producing DTAM waves and fictive advertisement calls, D-2-amino-5-phosphonopentanoic acid (DAPV or, simply, APV; Sigma) was either bath-applied (to intact and transected brains) or locally injected into DTAM bilaterally.

In bath-application experiments, 5-HT-induced DTAM LFP and motor nerve activity were recorded three times: *1*) in the absence of APV (control), *2*) following 15 min incubation in APV (50 μM, intact; 50 and 500 μM, transected), and *3*) after ≥1 h of washout in the absence of APV to confirm the reversibility of the APV effect. The 15 min incubation prior to 5-HT application ensured complete penetration of APV through the tissue.

In local injection experiments, 5-HT was applied 2 min after APV injection. Direct APV injections into DTAM eliminated the need to wait for drug diffusion through the tissue. For local injection, we used single barrel glass pipettes (1.5 mm OD, 0.86 mm ID; Harvard Apparatus, Holliston, MA) pulled on a Sutter Instrument P-97 Puller (Novato, CA), broken back to an approximately 10–15 μm tip, and filled with a solution of APV (0.5 or 1 mM in saline) and 5% fluoro-ruby (FR; tetramethylrhodamine dextran, 10,000 MW; Invitrogen, Carlsbad, CA). APV/FR was pressure injected bilaterally into DTAM (Pressure System IIe; Toohey, Fairfield, NJ). Brief injection pulses (10–20 ms, 20–30 psi) were applied (~5 Hz) until FR could be seen below the cerebellum surface (in DTAM) through a stereoscope. In several cases, we estimated the volume injected by later injecting the same number of pulses into mineral oil (based on the radius of the resulting red aqueous sphere); the average injection volume was estimated to be 18.9 ± 9.6 nl. 5-HT was bath-applied 2 min following the injection and fictive vocalizations in the laryngeal nerve were recorded. Control injections (FR in saline) were made to verify that physical perturbation and FR do not affect 5-HT-induced fictive vocal patterns. Only one bilateral injection (500 μM APV, 1,000 μM APV, or FR control) was made in each brain so the injection position could be later confirmed. Data were included for analysis only if 5-HT application elicited normal fictive advertisement calling after 1 h of recovery following APV or control injections. After each experiment, brains were fixed in 4% paraformaldehyde solution and sectioned horizontally to confirm that FR filled DTAM.

Analysis of vocalizations

We measured the fast and slow trill durations from 10 randomly selected calls at each temperature from all 10 animals using Raven software (Cornell Lab of Ornithology, Ithaca, NY). Sound frequency analyses showed that fast trill clicks lack a low-frequency (~1.25 kHz) component present in slow trill clicks (Yamaguchi et al. 2008). This allowed us to unambiguously distinguish trill boundaries. Trill durations were defined as the time between the first and last clicks of each trill; call durations were defined as the time between the first fast trill click and the last slow trill click. Introductory phases were observed only at the beginning of call renditions in vocal recordings

(see following text) and were thus excluded from in vivo analyses. Temperature coefficients (Q_{10}) were calculated for call and trill durations and compared with values obtained in vitro (see *Statistical analyses*).

Analysis of in vitro fictive vocalizations: slow trill, fast trill, and introductory phase

Duration of slow trill, fast trill, and introductory phase were measured to examine the function of pattern generators within the vocal CPG. For whole-brain temperature experiments, recordings were used for analyses if the following criteria were satisfied: calling was elicited by 5-HT at three or more temperatures and at least six consecutive calls were produced with the silent intervals between calls <1 s.

Both in vivo and in vitro, there is some variation in the structure of advertisement calls. The fictive calls always contained fictive fast trills, but some fictive calls within a series of consecutive calls contained either very short or no fictive slow trills. When we encountered these in our recordings, fictive slow trills were included in analyses only if they contained five or more CAPs; if there were fewer than five fictive slow trill CAPs or no fictive slow trills, we analyzed only fictive fast trills. As a consequence, the number of fictive slow trills used for analysis was lower than that of fictive fast trills. In addition, some advertisement calls are preceded by an introductory phase, a trill characterized by low-amplitude clicks at a slow repetition rate (~20–40 Hz; Fig. 1*A*). In vivo, introductory phases are typically included in the first few initial calls (but not in later calls) within a series of advertisement calls, whereas in vitro, most calls contain fictive introductory phases regardless of the call order within a series of fictive advertisement calls. When present, fictive introductory phases were also used for analyses.

Although the distinction between the fictive fast and slow trills was marked by a sudden reduction in the CAP amplitude and elongation in inter-CAP interval, the distinction between the fictive introductory phase and fast trill was less obvious. Instead, fictive vocal production transitions from introductory phase to full advertisement call in a swift but continuous progression. Here, we developed a quantitative method for defining fictive introductory phases and fast trills in vitro, to make accurate measurements of the fictive fast trill and introductory phase durations. Because introductory phases and fast trills are characterized by two factors—rate and amplitude of the CAPs—we calculated the product of instantaneous rate and amplitude, r*a (with the amplitude corresponding to the second of two CAPs used to calculate instantaneous frequency). Values of r*a were calculated for all fictive introductory phase and fast trill intervals, normalized to the maximum r*a, and plotted in a frequency histogram (bin width = 5%); each bin was then averaged across all preparations to produce a final histogram ($n = 11$; Fig. 1*B*). The resulting distribution showed one peak around 80% (representing fast trill intervals) with the rest skewed toward 0% (representing introductory intervals; Fig. 1*B*). The data plotted on a log-transformed *x*-axis histogram (50 bins/decade) were used to fit a two-term Gaussian curve to the resulting histogram (not shown) and the resulting μ values and σ values were taken as estimates for the mean and variance of fictive introductory phase ($\mu_1 \pm \sigma_1$) and fast trills ($\mu_2 \pm \sigma_2$). We defined $\mu_2 - 3\sigma_2$ (50% of maximum r*a) as the cutoff between introductory and fast trill intervals and the method was used to distinguish fictive introductory phase and fast trills in all analyses (Fig. 1*C*).

The timing of CAPs was determined using threshold search in Clampfit (Molecular Devices) for ≤10 calls per treatment. Instantaneous CAP rates were then calculated and assigned as fictive fast, slow, or introductory trills as described earlier. Maximum sustained CAP rates were calculated as the largest average of five consecutive intervals measured for each series of 5-HT-induced call intervals. The durations of the fictive introductory phase, fast trill, and slow trill were calculated as the time between the onset of the first and last CAPs within each fictive phase/trill. Total fictive call duration was defined as the time between fictive fast trill onset and slow trill offset (excluding the introductory phase). Intercall intervals were defined as the time between the onsets of two consecutive fictive fast trills.

Analysis of LFP recordings

The timing and temporal structure of the DTAM LFP waves were analyzed and the extents of their concurrence with fast trills were examined. For temperature manipulation studies in transected brains, recordings were included in analyses if at least six LFP waves were recorded at each of three temperatures in each preparation. Extracellular traces obtained from DTAM were first low-pass Gaussian filtered (5 Hz) to remove high-frequency signals. Timings of onset and offset of the wave were defined as follows. The first (f') and second derivative (f'') of the filtered trace were first obtained. The time of the largest f'' peak per wave cycle was defined to be the offset. The onset of the wave was defined to be the time of the second largest peak of f'' within 0 to 250 ms preceding the maximum f' peak (peak slope of the rising phase of the wave). Onset and offset timings were later visually confirmed. The area of the wave was calculated from the low-pass filtered trace, measured between the times of onset and offset.

Call and LFP wave interval analyses

Call and LFP wave intervals were also analyzed to assess temporal organization of pattern generation. Typically, fictive calls (intact brains) and LFP waves (intact and transected brains) occur in series, with a frequency of approximately once/s. A series of fictive calls or waves can be separated from another series by intervals anywhere from about 2 s to >60 s. Intercall interval (time between the onset of two calls) and interwave interval (time between on offset of one wave and the onset of the next wave) are obtained from calls/waves within a series of calls/waves.

Statistical analyses

Temperature-dependent effects in pattern generation from in vivo vocal data were determined by comparing the call and trill durations obtained at two temperatures (18 and 26°C) within individuals using the Wilcoxon signed-rank test (average of 10 calls per treatment). To assess the in vitro temperature dependence of fictive call, trill (fast and slow), and wave durations, a median value was obtained from at least three temperatures for each animal. Linear regression lines were fit to the data for each individual to obtain a qualitative description of the temperature dependence. For quantitative analyses, mixed-model (fixed slope, variable intercept; individual as random effect) regressions were performed using JMP 8 software (SAS Institute, Cary, NC); models were computed using the restricted maximum likelihood method. The temperature coefficient Q_{10} was also calculated to quantify the degree of thermal sensitivity of each dependent variable. For positive correlations, $Q_{10} = (R_2/R_1)^{10}/(T_2 - T_1)$, where T_1 is the lowest temperature, T_2 is the higher temperature, and R is the dependent variable. For inverse relations, we calculated Q_{10} as $(R_1/R_2)^{10}/(T_2 - T_1)$. Differences between Q_{10} values obtained from whole-brain and transected brain experiments were tested using the Wilcoxon signed-rank test. Effects of APV on wave area (transected brains) and fictive fast trill rates (intact brains) were also tested using the Wilcoxon signed-rank test. To compare wave duration and interval Q_{10} values between intact and transected preparations, we used the unpaired Mann–Whitney *U* test. We also used the Mann–Whitney *U* test to compare trill durations of fictive and in vivo call parameters. Because APV and saline control injections had to be performed in unpaired samples (only one injection per brain was possible to allow anatomic verification of injection placement), the Kruskal–Wallis test with Dunn's multiple comparison test was used to determine whether APV injections reduced maximum CAP rates. To determine whether the frequency distribution of r*a values after APV injections were

different from those of controls, we used the Kolmogorov–Smirnov (K-S) test to compare frequency histograms. All data are reported as means ± SD unless otherwise noted.

RESULTS

Distinct activity patterns in DTAM correlate with fictive vocal rhythm and pattern

As a first step in understanding the neural mechanisms that regulate the timing of calls, we obtained LFP recordings from DTAM during 5-HT-induced fictive vocal production. The most robust vocal-related activity was recorded within previously identified DTAM coordinates (Brahic and Kelley 2003; Zornik and Kelley 2008). Because no additional vocal nuclei surround the region occupied by DTAM (Brahic and Kelley 2003; Kelley 1980; Wetzel et al. 1985), we conclude that the vocal-related activity recorded originated in DTAM.

Two primary patterns of activity were observed. First, LFP recordings revealed brief bursts of activity time-locked with each CAP (Fig. 2, *A–D*). Fast activity bursts occurred during all three fictive trills (introductory phase, fast trill, and slow trill); however, the largest amplitude of phasic activity was observed during fictive fast trills and introductory phase (Fig. 2, *B–D*). Although fictive slow trill CAPs have higher amplitude than that of fictive introductory CAPs in the motor nerves, the fictive slow trill–related activity in DTAM was smaller in amplitude (Fig. 2, *B* and *D*). In addition, phasic activity that precedes motor CAPs was observed during fictive introductory phase and fast trills (arrows, Fig. 2, *B* and *C*), but DTAM activity during fictive slow trills was either overlapping with or following motor CAPs (Fig. 2*D*). These results indicate that neuronal activities in DTAM during fictive introductory phase, fast trill, and slow trill are qualitatively different.

The second pattern revealed by LFP recordings was a slow baseline wave that occurs once per call (Fig. 2*A*). This wave consists of an upward baseline shift that peaks during fictive fast trill and ends during the fast-to-slow trill transition. We defined the onset and offset of the wave quantitatively (see METHODS). We examined the timing of fictive trills relative to the DTAM wave by plotting perievent time histograms (bins = 10 ms) using the delay between the onset and offset of waves and fictive trills recorded from each animal (20.0–20.9°C). Fictive fast trill onset almost always followed the beginning of waves with a mean delay of 226.4 ± 51.3 ms (Fig. 2*E*; $\mu \pm \sigma$ based on a Gaussian model fit to the histogram). Fictive fast trills typically ended before the wave offset with the mean interval of 42.5 ± 8.7 ms (Fig. 2*F*); this relation was more tightly correlated than the onset delay. Thus the LFP wave starts before and outlasts the fictive fast trill. Fictive slow trill onset was also tightly correlated with wave offset, normally beginning shortly after the end of the wave (13.4 ± 16.1 ms; Fig. 2*G*). Fictive slow trill offset, in contrast, was not closely linked with onset of the wave of the following fictive call (1,318.6 ± 203.7 ms; data not shown) but, importantly, waves of the following call cycle never began before the end of fictive slow trill. In contrast to tight relations between wave and fictive fast and slow trill, onset of fictive introductory phase was not normally distributed; values ranged between >3 s before wave onset and >100 ms after the beginning of a wave (Fig. 2*H*). These results suggest that the introductory phase is not correlated with wave production. Together, these data suggest that fast trills mostly occur during waves, whereas slow trills occur between waves.

LFP waves are endogenous to DTAM, whereas phasic activity requires connections between DTAM and n.IX–X

We have previously shown that transections between DTAM and n.IX–X eliminate fictive vocalizations (Rhodes et al. 2007). Here, we sought to determine whether LFP waves in DTAM also require connections with n.IX–X or whether they are endogenous to DTAM circuitry. Surprisingly, 5-HT-induced waves could still be elicited after transecting the connections between n.IX–X and DTAM (Fig. 3*A*). Transections just anterior of DTAM also did not eliminate waves (data not shown), indicating that midbrain and forebrain inputs are not required for DTAM wave generation. In contrast, the phasic activity in DTAM that correlates with vocal CAPs is eliminated entirely in transected brains; the remaining tonic bursts of activity coinciding with the waves are unpatterned and lack any trill-like rhythms (compare Figs. 2*C* and 3*B*). Thus the LFP wave seems to be generated endogenously within DTAM, whereas the phasic activity relies on intact connections between DTAM and n.IX–X.

Temporal profile of the DTAM wave is thermally sensitive

A previous study demonstrated that rhythm generation of the vocal CPG is temperature dependent; during fast and slow trills, click rates become faster at warmer temperatures (Yamaguchi et al. 2008). Here we addressed whether the endogenous DTAM wave also depends on temperature. To this end, we performed temperature manipulations in brains transected between DTAM and n.IX–X and analyzed the temporal profile of DTAM waves at various temperatures. The results showed that the wave durations and intervals are temperature dependent (see example traces in Fig. 3*C*). Regression lines of wave duration data for all eight individuals had negative slopes (Fig. 3*D*). Likewise, all interwave interval regression lines showed a negative correlation with temperature (Fig. 3*E*). Mixed-model regressions verified that temperature significantly accounted for wave duration (slope = −35.9 ± 4.3 ms, t ratio = −8.45, $P < 0.0001$) and interwave interval (−140.9 ± 13.9, t ratio = −10.14, $P < 0.0001$). Q_{10} values for wave data were large: 2.5 ± 0.6 (duration) and 4.2 ± 0.9 (interval). These results indicate that the temporal profile of endogenous DTAM waves relies on the rate at which neuronal processing takes place within DTAM. Furthermore, high Q_{10} values suggest the involvement of synaptic transmission for the generation of DTAM waves (Janssen 1992).

Temporal patterns of vocalizations are temperature dependent

Because DTAM waves are correlated with the onset and offset of fictive trills, we hypothesized that the DTAM wave dictates the temporal patterns of calls. The hypothesis predicts the temperature sensitivity of the DTAM wave should translate into temperature-dependent call and trill durations.

When vocalizations from 10 males were recorded at both warm (26°C) and cool (18°C) temperatures, call and trill durations showed significant temperature dependence (Fig. 4*C*). Call duration, intercall intervals, and fast trill and slow trill durations were all significantly longer at 18°C than those at 26°C,

with Q_{10} values ranging from 1.7 to 2.6 (Table 1). Introductory phases were not analyzed because they were infrequent in vivo (see METHODS). Thus the call and trill durations depend on ambient temperature in vivo.

Similarly, when fictive advertisement call and trill durations recorded at three or four distinct temperatures (range, 15.6–23.6°C) were analyzed, all 11 preparations showed significant temperature dependence. Fictive call duration, intercall inter-

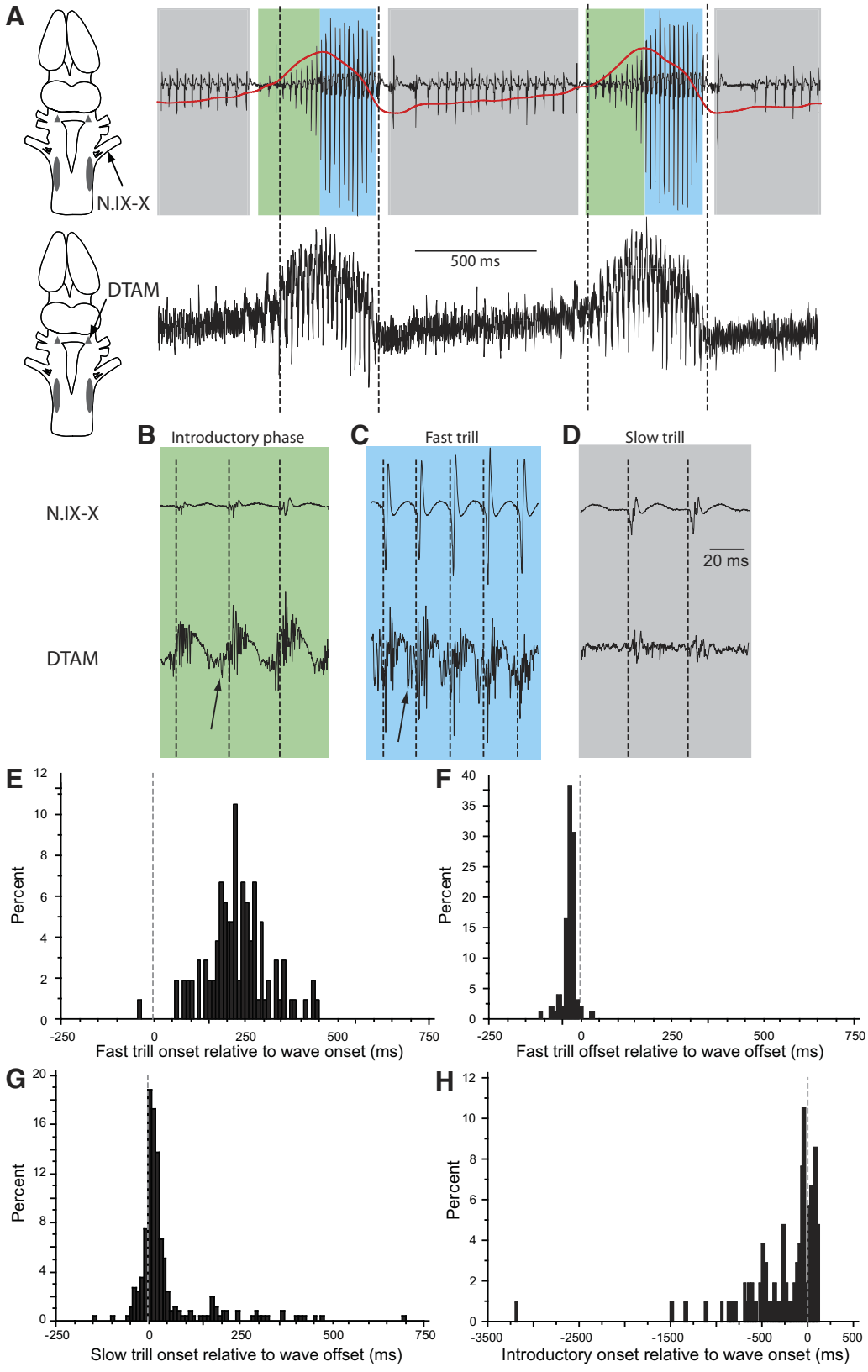

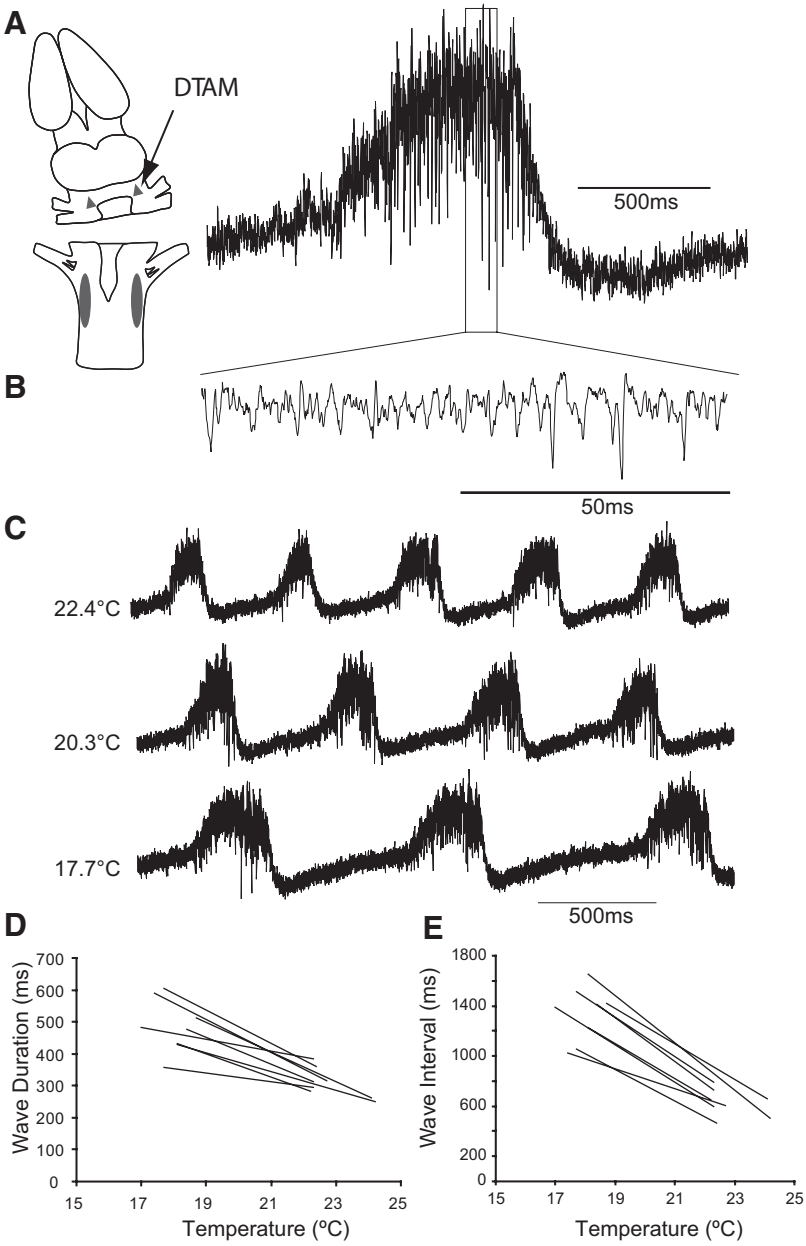

FIG. 3. LFP waves are endogenous to DTAM and thermally sensitive. *A*, *left*: diagram of a brain transected between DTAM (gray triangles) and n.IX–X (gray ovals); arrow points to the recording site in DTAM. *Right*: example recording of a single serotonin (5-HT)-induced LFP wave recorded in DTAM following transection between DTAM and n.IX–X. Trace shows high-frequency activity overlying the slow wave. *B*: expanded higher-resolution view of trace from *A*; unlike phasic activity in the intact brain, this high-frequency activity is unpatterned. *C*: example traces of 5-HT-induced endogenous DTAM waves at 3 distinct temperatures. Note that both wave durations and wave intervals become elongated at colder temperatures. *D* and *E*: regression lines of data from individual preparations demonstrate that the wave durations (*D*) and intervals (*E*) vary inversely with temperature.

val, and fast and slow trill durations all became longer when the brains were held at a cooler temperature. Linear regression lines fitted to total fictive call duration data all had negative slopes ($n = 11$; Fig. 5*B*) and those fitted to fictive slow trill, fast trill, and intercall interval exhibited negative slopes for 10 of 11 preparations (Fig. 5*B*). In contrast, only 3 of 11 regressions of fictive introductory phase durations were negative (Fig. 5*B*). Quantitative analyses of the temperature dependence of fictive call and trill duration using mixed-effects regression analyses (temperature as fixed effect, individual as random

FIG. 2. A slow local field potential (LFP) wave in DTAM correlates with fictive fast trills. *A*: example nerve (*top trace*, black) and DTAM (*bottom trace*) recordings showing 2 fictive advertisement calls; a low-pass (5 Hz) filtered trace (red) of the DTAM recording is shown overlaid on the nerve recording. The recording sites are indicated by arrows on dorsal view of the brains on the *left* (DTAM and n.IX–X are indicated by gray triangles and gray ovals, respectively). The dotted lines illustrate the onset and offset of the wave relative to each fictive vocal phase. In this example, a short fictive introductory phase is present and the wave onset occurs shortly after the call begins. The fictive fast trill ends before the end of the wave. *B–D*: expanded temporal views of N.IX–X (*top*) and DTAM (*bottom*) traces show the phasic activity in DTAM roughly coinciding with nerve CAPs during fictive introductory phase (*B*), fast trill (*C*), and slow trill (*D*). Phasic DTAM activity with the largest amplitude occurs during fictive fast trill. Also, note that phasic DTAM activity during fictive introductory phase is larger than that during fictive slow trill, despite the fact that fictive slow trill CAPs are larger than fictive introductory CAPs. Dotted lines mark the time of CAP onset; note that phasic activity during fictive introductory phase (*B*) and fast trill (*C*) precede and follow CAP onset (arrows), whereas DTAM activity during fictive slow trill (*D*) only follows CAP onset. *E*: frequency histogram showing the delay between wave onset and fictive fast trill onset. Gray dotted line indicates wave onset (*time = 0*). *F*: histogram plotting the time of fictive fast trill offset relative to wave offset (gray dotted line). *G*: histogram plotting the time of fictive slow trill onset relative to wave offset (gray dotted line). *H*: frequency histogram plotting the time of fictive introductory phase onset relative to wave onset (gray dotted line).

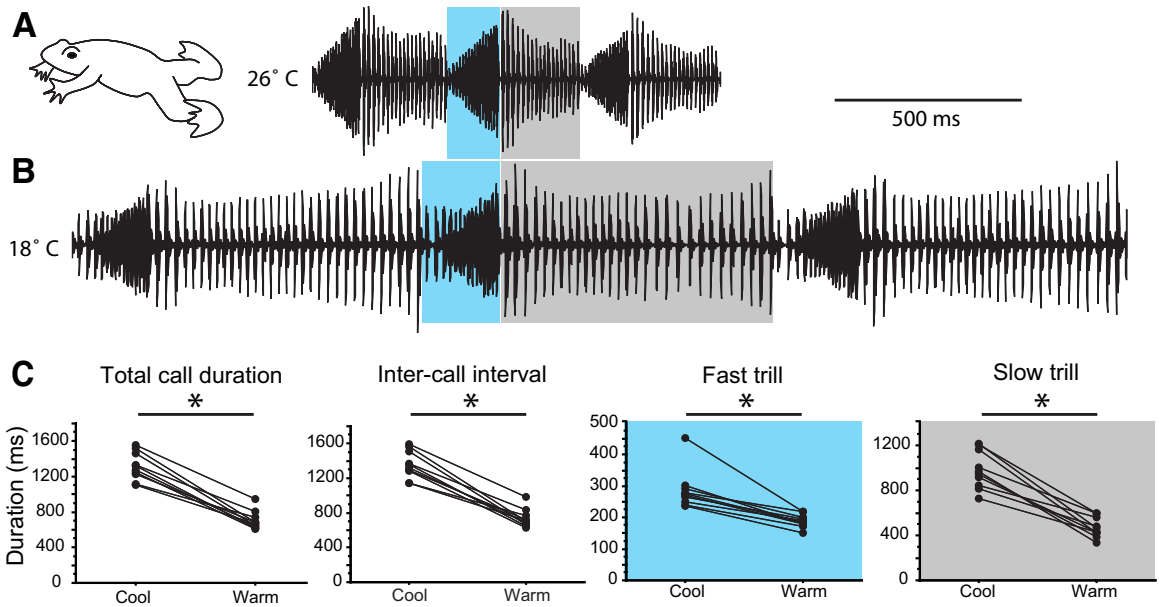

FIG. 4. Vocalizations are thermally sensitive. *A*: sound oscillogram of 3 male advertisement calls made by intact frogs. Calls consist of alternating fast (blue) and slow (gray) trills. Frogs kept in warm (26°C) aquaria produce advertisement calls with shortened call and trill durations compared with those of frogs in cooler (18°C) environments (*B*). *C*: summary charts showing call duration, intercall interval, fast trill duration, and slow trill duration at cool and warm temperatures. Dots indicate median for each individual ($n = 10$) recorded at each temperature, connected by lines. *$P < 0.005$; Wilcoxon signed-rank test.

effect, fixed slope, variable intercept) confirmed these findings, as did Q_{10} values (Table 2). Thus we conclude that the durations of all fictive call parameters measured in vitro, except for introductory phase, are thermally sensitive.

Variation in DTAM wave duration explains variation in fictive call duration

We next examined how DTAM waves respond to temperature in intact brains and how the duration of the waves covary with the fictive trill durations. The duration of DTAM waves recorded from all 11 intact brain preparations (the same set as used to test thermal sensitivity of fictive vocalizations described earlier), each recorded at three or four distinct temperatures, showed an inverse correlation with the temperature (as did waves generated by a transected brain). Regression lines fitted to DTAM wave duration had negative slopes in 9 of 11 preparations (Fig. 5*C*). Although the wave duration Q_{10} (1.7 ± 0.5) was significantly lower than that obtained from the transected brain ($z = -2.312$, $P = 0.021$; Mann–Whitney *U* test), it was not statistically different from fictive fast trill duration Q_{10} ($z = -0.248$, $P = 0.804$; Mann–Whitney *U* test). A mixed-model regression revealed a slope of −20.6 ± 3.9 ms (t ratio = −5.26, $P < 0.0001$), confirming that wave duration is inversely proportional to temperature as it is in transected brains.

Importantly, the DTAM wave duration significantly accounted for the fictive fast trill duration. Regression lines comparing fast trill duration versus wave duration showed a positive correlation in 9 of 11 preparations (Fig. 5*D*). A mixed-model regression analysis (fictive fast trill duration as the dependent variable, wave duration as the independent factor) confirmed that the wave duration significantly accounted for the duration of fictive fast trills (slope = 0.53 ± 0.08, t ratio = 6.45, $P < 0.0001$). Similarly, fictive slow trill duration could be explained by the interwave interval. Because fictive slow trills occurred only between waves, we examined the relation between fictive slow trill durations and interwave intervals; linear regression results revealed a positive correlation in 10 of 11 preparations (Fig. 5*E*). Mixed-model regression analysis (dependent variable, fictive slow trill duration; independent variable, interwave interval) showed that the duration of fictive slow trills could be partially explained by interwave intervals (slope = 0.51 ± 0.08, t ratio = 6.29, $P < 0.0001$). In contrast to the tight association between the fictive fast trill and wave duration, the duration of fictive introductory phase could not be explained by the wave duration (slope = −0.50, t ratio = −1.23, $P = 0.23$; data not shown).

Thus the durations of both DTAM waves and fictive calls covary with the temperature of the CNS across a wide range.

TABLE 1. *Duration of advertisement calls recorded in vivo at two distinct temperatures*

Call Duration Parameters	Duration, ms		Test Statistic	*P* Value	Q_{10} Value
	At 18°C	At 26°C			
Total call	1,317 ± 158	703 ± 104	$z = -2.803$	0.005	2.2 ± 0.4
Intercall interval	1,357 ± 158	735 ± 106	$z = -2.803$	0.005	2.2 ± 0.4
Fast trill	286 ± 63	189 ± 21	$z = -2.803$	0.005	1.7 ± 0.3
Slow trill	984 ± 170	470 ± 89	$z = -2.803$	0.005	2.6 ± 0.8

Values are means ± SD.

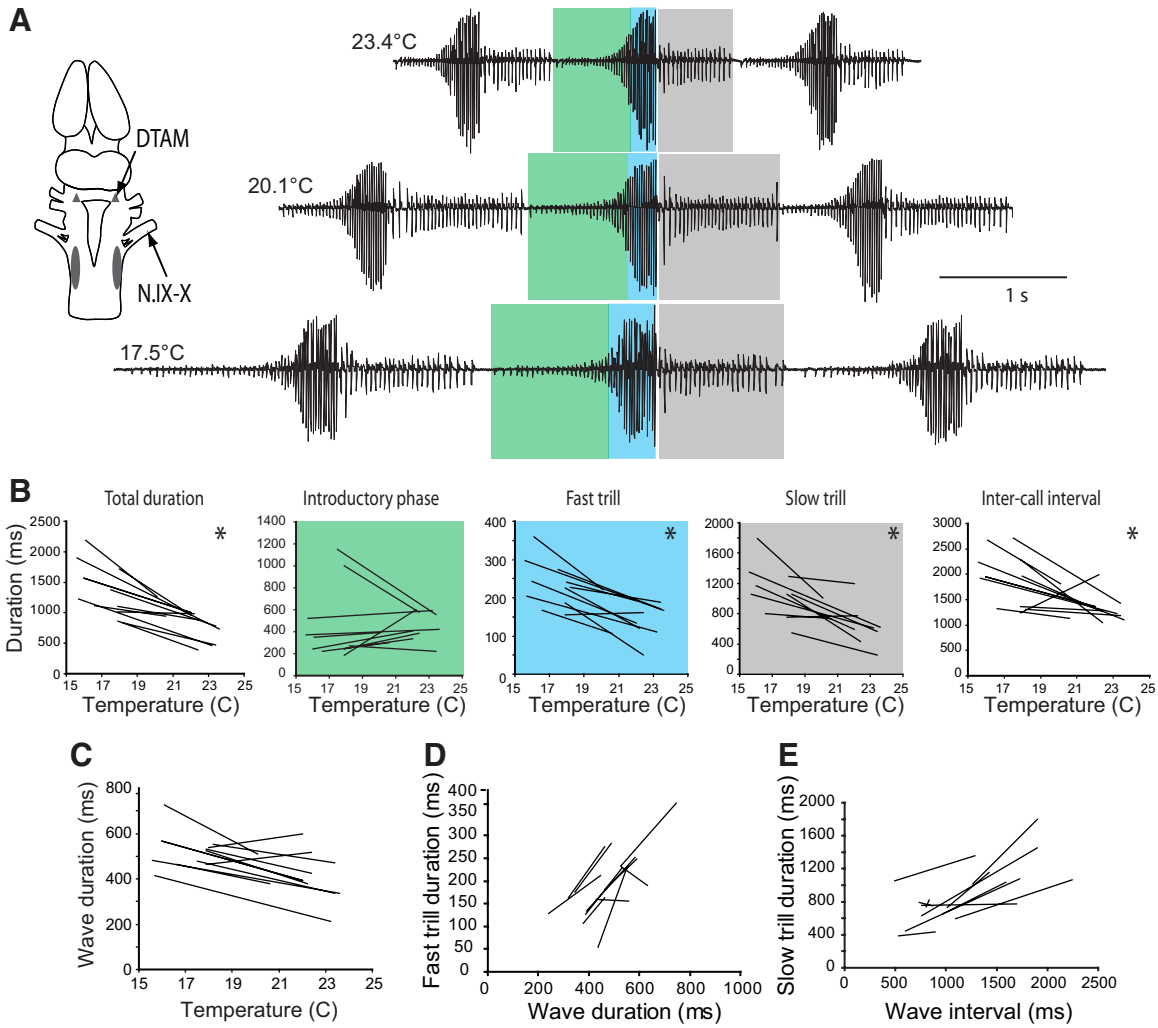

FIG. 5. Fictive vocalizations are temperature sensitive. *A*, *left*: diagram of intact isolated brain; arrow points to recording sites N.IX–X and DTAM. DTAM is indicated by gray triangles and gray ovals represent n.IX–X. *Right*: example recordings of fictive vocalizations evoked at 23.4, 20.1, and 17.5°C. The 3 fictive trills—introductory, fast, and slow—are color-coded in the middle call of each trace, as in previous figures. *B*: summary charts showing linear regression trend lines for each of 11 preparations. Most lines describing fictive total call (11 of 11), fast trill (10 of 11), slow trill (10 of 11), and intercall interval (10 of 11) durations have negative slopes; only 3 of 11 regression lines for fictive introductory phase, however, show a negative trend. Asterisks in the *top right corner* of each panel denote mixed-model regression with significant correlation between call parameter and temperature. *C*: linear regression trend lines of wave duration vs. temperature show negative slopes in 9 of 11 preparations. *D*: linear regressions of fictive fast trill durations vs. wave duration reveal positive relations in 9 of 11 preparations. *E*: linear regressions show a positive relations (in 10 of 11 preparations) between fictive slow trill durations and wave intervals.

Furthermore, the mixed-model regressions indicate that a doubling of the wave duration and interwave interval corresponds with a roughly 50% increase in fast and slow trill durations, respectively.

DTAM temperature affects timing of vocal patterns

The close correlation of the DTAM wave and fictive trill durations over a wide range is consistent with the hypothesis that the DTAM wave determines the trill duration. Although temperature changes to the whole brain significantly altered call durations, we sought to verify that this was the result of altered temporal profile of the DTAM waves, not another region of the CPG. To this end, we induced changes in the DTAM wave by selectively controlling the temperature of DTAM in vitro. As a control, we also manipulated the temperature of n.IX–X and examined its effect on call duration.

TABLE 2. *Temperature coefficients of fictive advertisement call durations*

Call Duration Parameters	Q_{10} Value	Mixed-Model Coefficient (±SE), ms	*t* Ratio	*P* Value
Total call	3.2 ± 2.2	−85.4 ± 13.0	−6.56	<0.0001
Introductory phase	1.1 ± 1.1	−0.5 ± 0.4	−1.23	=0.23
Fast trill	2.9 ± 1.9	−16.0 ± 2.6	−6.16	<0.0001
Slow trill	2.6 ± 1.4	−76.7 ± 11.8	−6.50	<0.0001
Intercall interval	2.2 ± 1.3	−108.9 ± 23.5	−4.63	<0.0001

Values are means ± SD.

TABLE 3. *CAP rates while temperatures of DTAM and n.IX–X are selectively manipulated compared with those recorded under control conditions*

Call Duration Parameter	CAP Rates, Hz			DTAM Versus Control		n.IX–X Versus Control	
	DTAM Cooling	Control	n.IX–X Cooling	Test Statistic	*P* Value	Test Statistic	*P* Value
Fast trill	55.3 ± 5.6	61.6 ± 6.3	57.4 ± 6.1	$z = -2.201$	=0.028	$z = -2.201$	=0.028
Slow trill	28.8 ± 5.5	34.3 ± 5.5	31.5 ± 3.3	$z = -2.201$	=0.028	$z = -1.782$	=0.075
Introductory phase	41.7 ± 8.7	49.6 ± 8.5	45.8 ± 10.2	$z = -2.201$	=0.028	$z = -1.992$	=0.046

Values are means ± SD.

Because DTAM and n.IX–X are spatially segregated, we were able to selectively cool each nucleus in turn while keeping the other at room temperature. We then compared these recordings of fictive calls with a final control in which both nuclei were at room temperature.

In a previous study, we showed that cooling DTAM using cryoprobes slowed CAP rates of both slow and fast trills (Yamaguchi et al. 2008). In this study, we were able to replicate our initial findings using the new split-dish selective cooling technique. Cooling the DTAM portion of the brain decreased CAP rates for fictive fast trill, slow trill, and introductory phases (Table 3). Unlike the previous study, we were also able to selectively cool n.IX–X using our new technique (see METHODS). These experiments showed that n.IX–X cooling significantly reduced fictive introductory phase and fast trill CAP rates; fictive slow trill rates were reduced in five of six preparations, although this difference was not significant (Table 3). Taken together, we conclude that DTAM and n.IX–X both contain rhythm generating circuits that control advertisement call CAP rates.

When DTAM was selectively cooled, the durations of 5-HT-induced fictive vocalization were also altered. Total fictive call duration, intercall interval, and fast trill durations were all significantly increased in response to selective cooling of DTAM (Fig. 6*A*; $n = 6$; Table 4). However, the durations of fictive slow trill and introductory phase were not significantly elongated by selective cooling of DTAM (Fig. 6*A*; Table 4). Thus although controlling the temperature of the whole brain affects both fictive fast and slow trills, selective cooling of DTAM has the most prominent effect on fictive fast trill durations.

When n.IX–X was selectively cooled, in contrast, no fictive vocal durations were significantly different from those recorded under control conditions (Fig. 6*B*; $n = 6$). This is apparent in total fictive call duration, intercall interval, fast trill duration, slow trill duration, and introductory phase (Table 4). These results indicate that DTAM is the main determinant of call durations within the vocal CPG; reducing the rate of neuronal processing within DTAM by lowering the temperature, and thus elongating the DTAM LFP wave, resulted in elongating the fictive fast trill and, consequently, call duration.

DTAM waves require NMDAR signaling

How are the LFP waves generated by the neurons within DTAM? As a first step in addressing this question, we attempted to eliminate the DTAM wave by blocking synaptic transmission using pharmacological agents. Specifically, we suspected the involvement of the NMDAR in regulating the trill and call duration because of its role in coordinating the motor patterns over similar timescales in many other systems (Collingridge et al. 1988; Daw et al. 1993; Smith et al. 2000).

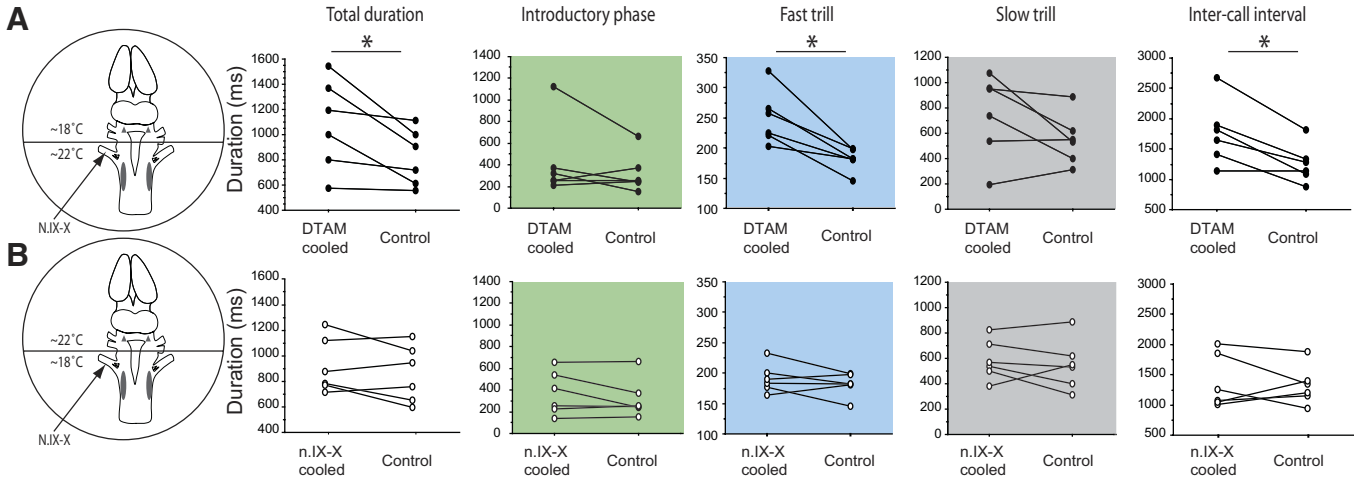

FIG. 6. Selective cooling of DTAM and n.IX–X. *A*: Left, diagram of an isolated brain in a dual chambered recording dish. In these experiments, the DTAM-containing chamber was kept at about 18°C, whereas the n.IX–X-containing chamber was kept at roughly 22°C. Right, summary graphs of fictive trill and call durations comparing data from DTAM cooling (left data points) and control treatments (both chambers at ~22°C; right data points). Selectively cooling DTAM elongates fictive fast trills and call durations. Asterisks denote statistically significant differences between the treatments. *B*, *left*: illustration of the experimental treatment, with the brain region containing n.IX–X cooled to about 18°C and the DTAM portion held at close to 22°C. *Right*: summary graphs comparing fictive call durations during n.IX–X cooling and control recordings; none of the parameters is statistically different between n.IX–X cooling and control conditions.

TABLE 4. *Call duration while temperatures of DTAM and n.IX–X are selectively manipulated compared with those recorded under control conditions*

Call Duration Parameter	DTAM Cooling	Control	n.IX–X Cooling	DTAM Versus Control		n.IX–X Versus Control	
				Test Statistic	*P* Value	Test Statistic	*P* Value
Total call	1,080 ± 362	818 ± 222	880 ± 215	$z = -2.201$	=0.028	$z = -0.943$	=0.345
Introductory phase	423 ± 349	322 ± 181	371 ± 201	$z = -1.153$	=0.249	$z = -0.314$	=0.753
Fast trill	250 ± 45	181 ± 19	191 ± 24	$z = -2.201$	=0.028	$z = -0.943$	=0.345
Slow trill	742 ± 329	549 ± 199	588 ± 158	$z = -1.363$	=0.173	$z = -0.734$	=0.463
Intercall interval	1,763 ± 526	1,257 ± 318	1,310 ± 445	$z = -1.992$	=0.046	$z = -0.314$	=0.753

Values are means ± SD.

To test this possibility, we first bath-applied the NMDAR antagonist APV to the transected brains and examined its effects on the 5-HT-induced DTAM wave. We found that APV strongly inhibits production of DTAM waves generated by the transected brains (Fig. 7, *A* and *B*). With 50 μM APV, the wave area (see METHODS) was significantly reduced to 33.9 ± 22.2% of control ($n = 5$, $z = -2.023$, $P = 0.043$); 1 h after washout of APV, the wave area (141.3 ± 89.5%) was similar to that of control ($n = 5$, $z = -0.674$, $P = 0.500$). At a higher concentration (500 μM), waves were completely eliminated in four of five preparations; overall, the average area during 500 μM APV application was only 6.2 ± 13.8% of control levels ($n = 5$, $z = -2.023$, $P = 0.043$), whereas the mean area returned to 85.7 ± 44.6% after 1 h of washout, a value similar to that of control ($n = 5$, $z = -0.674$, $P = 0.500$). Thus we conclude that APV blocks endogenous DTAM waves generated by transected brains, suggesting that glutamatergic transmission mediated by NMDARs is required for producing waves.

Fast trill production requires functional NMDARs in DTAM

Because APV disrupted DTAM waves in the transected brain, we next tested whether blocking DTAM waves in the intact (whole) brain would abolish fictive fast trill production. To this end, we preincubated intact brains with 50 μM APV to assess its effect on 5-HT-induced DTAM wave and nerve activity. We first confirmed that the application of APV completely blocked the DTAM wave ($n = 4$) as in transected brains (Fig. 7*C*). We discovered that APV completely blocked normal fictive fast trill production in all preparations tested ($n = 7$, Fig. 6, *C* and *D*). Maximum sustained CAP rates during APV application (8.7–28.2 Hz) were well below normal fictive fast trill rates and were significantly lower than CAP rates obtained during control (50.5–62.0 Hz; $z = -2.366$, $P = 0.018$) and recovery (52.6–63.0 Hz; $z = -2.366$, $P = 0.018$), whereas control and recovery values were not statistically different ($z = -1.521$, $P = 0.128$). Thus when DTAM waves are blocked by APV, fictive fast trill was also eliminated.

DTAM and nerve recordings during APV treatment showed activity that closely resembles the fictive introductory phase (relatively large activity in DTAM preceding and following each CAP), but not similar to fictive slow trill (Fig. 7*E*). When the frequency distribution of r∗a values (rate times amplitude for each interval; index values used to distinguish fictive introductory phases and fast trills; see METHODS) before and during APV application were plotted, we found that the component that constitutes fictive fast trill (>50% maximum r∗a) in the control distribution is entirely eliminated from the APV distribution (Fig. 7*F*). Accordingly, overall frequency distributions were significantly different (maximum difference = 0.900, $P < 0.0001$, K-S test). These results suggest that blocking LFP wave activity might eliminate fast trills by preventing the transition from introductory phase into fast trill. Fictive slow trill was also not generated, perhaps because slow trill initiation requires inputs from the fast trill circuit.

Finally, we tested whether bath-applied APV was acting directly in DTAM to eliminate fictive fast trills. To achieve this goal, we performed bilateral injections of APV (or saline for control) into DTAM before eliciting 5-HT-induced fictive vocalizations. Bilateral injections of 500 μM APV decreased the occurrence of fictive fast trills and increased the incidence of fictive introductory phase, although maximum sustained CAP rates did not significantly differ from control values (APV: 0–53.3 Hz, $n = 8$; control: 57.6–68.1 Hz, $n = 4$; rank-sum difference = −6.875, $P > 0.05$; Fig. 8*A*). However, the distribution of r∗a values in APV injected preparation significantly differed from control (Fig. 8*C*; maximum difference = 0.750, $P < 0.0001$, K-S test). We next used a slightly higher concentration of 1 mM APV, in case the previous injection was not sufficient to silence all NMDARs in DTAM. In response to this higher dose of APV injections into DTAM, fictive fast trills were eliminated in all cases and maximum sustained CAP rates were significantly reduced compared with controls (Fig. 8*A*; $n = 6$, range = 0.7–16.2 Hz, rank-sum difference = −11.83, $P < 0.05$). Accordingly, the frequency distribution of r∗a values differed significantly from those of control (Fig. 8*B*; maximum difference = 0.950, $P < 0.0001$, K-S test). Injections of saline, however, did not alter the r∗a frequency distribution, showing the full range of fictive introductory- and fast trill-like intervals (Fig. 8*D*; maximum difference = 0.200, $P = 0.899$, K-S test). Thus we conclude that the effect of APV on the fictive vocalizations was mediated by its action in DTAM. Taken together, these data support the argument that NMDAR-sensitive neuronal processing within DTAM (recorded as LFP waves) is required for fast trill production and may therefore regulate the timing of calls.

DISCUSSION

Identifying distinct rhythm and pattern generators in a vocal CPG

Advertisement calls of *X. laevis* males are rhythmic and temporally modulated. Thus the function of the CPG can be divided into two distinct temporal scales. On a shorter "rhythm generator" timescale, the CPG controls the rates of fast (60 Hz) and slow (30 Hz) trills. On a longer "pattern generator"

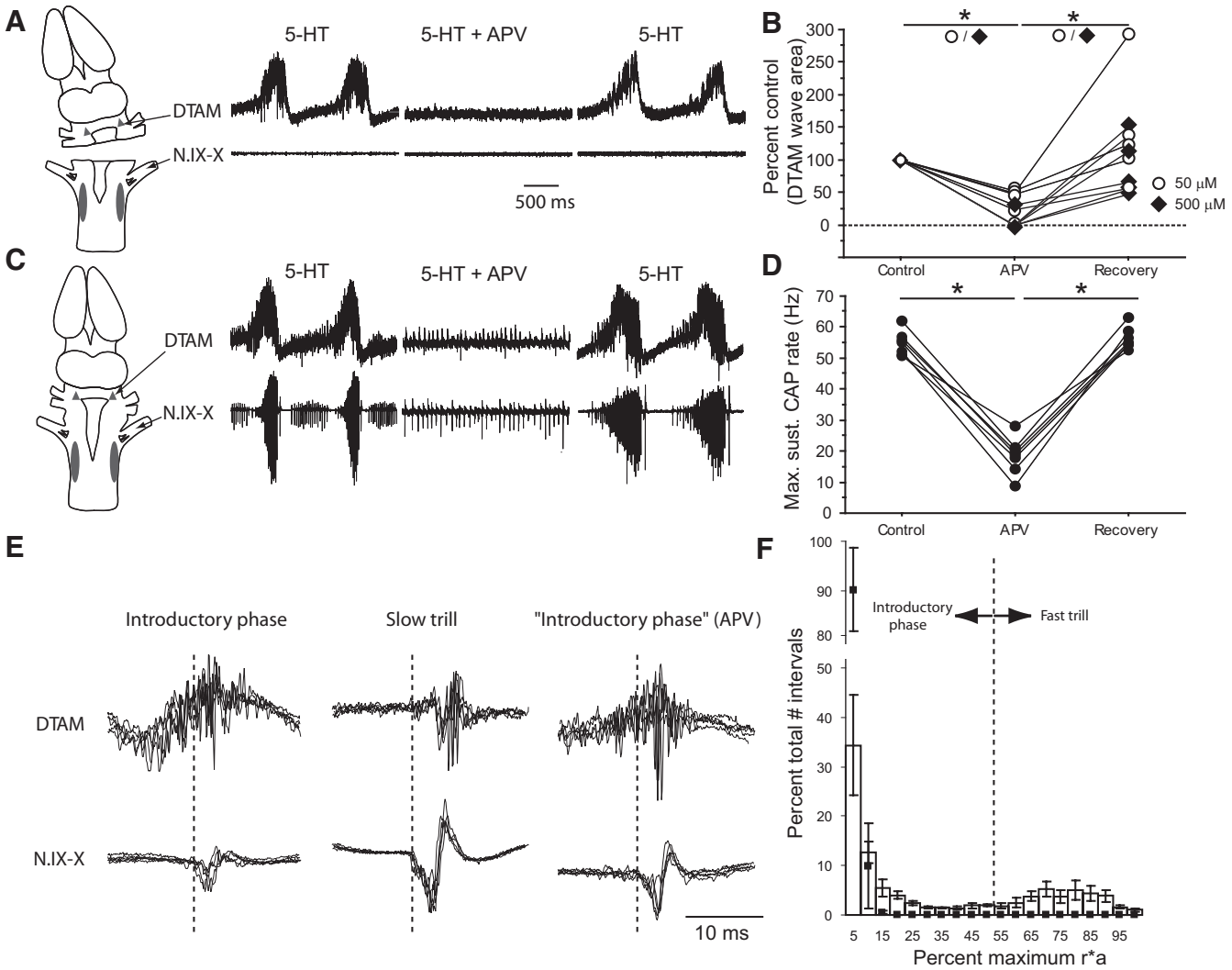

FIG. 7. DTAM waves and fictive fast trills require functional *N*-methyl-D-aspartate receptors (NMDARs). *A*: diagram on the *left* shows dorsal view of the brain with the plane of transection indicated (DTAM as gray triangles; n.IX–X as gray ovals). In transected brains, DTAM waves induced by 5-HT application (*left trace*) can be blocked by adding NMDAR antagonist D-2-amino-5-phosphonopentanoic acid (DAPV or, simply, APV) to the bath (*center trace*); after 1 h of washout, waves can once again be elicited (*right trace*). *B*: graph summarizing effects of 2 APV concentrations on the DTAM wave area: 50 μM APV (open circles) results in a significant, reversible reduction in wave area; 500 μM APV (filled diamonds) reversibly blocked all waves in 4 of 5 preparations (the average area of the remaining preparation was reduced to 31% of control); $^*P < 0.043$, Wilcoxon signed-rank test. *C*, *left*: diagram showing intact brain as recorded in the traces to the *right*. Example of DTAM waves (*top traces*) and fictive advertisement calls (*bottom traces*) induced by 5-HT (*left traces*). When 50 μM APV is incubated in the bath before 5-HT application, only low-amplitude, low-rate fictive introductory CAPs are produced and DTAM waves are eliminated (*middle traces*). Waves and fictive advertisement calls are reinstated 1 h after washing APV from the bath (*right traces*). *D*: summary graph showing maximum sustained CAP rates before, during, and following APV coapplication with 5-HT. $n = 7$, $^*P < 0.018$; Wilcoxon signed-rank test. *E*: 5 overlaid traces of phasic LFP activity in DTAM (*top*) and fictive nerve CAPs (*bottom*) during fictive introductory (*left*) and slow trill (*center*) CAPs during 5-HT-induced fictive calling. The recordings on the *right* show activity during 5-HT/APV application; DTAM recordings and nerve CAPs (5 overlaid traces of each) both resemble activity during fictive introductory phase. Dotted lines indicate CAP onset in each example. *F*: frequency histogram comparing the distributions of r*a values for 5-HT-induced calling during control (open bars) and APV (black squares) conditions.

timescale, the CPG sets the duration of each trill (200 and 800 ms, respectively). In this study, we discovered neural correlates of both vocal rhythm and pattern in DTAM.

Previous investigations have shown that intact connections between DTAM and n.IX–X are necessary for producing fictive vocalizations (Rhodes et al. 2007) and anatomical experiments indicate a strong degree of connectivity between the two regions (Zornik and Kelley 2007). In this study, we identified neural correlates of trill rhythm in DTAM (phasic bursts) that accompany vocal CAPs. Like CAP production, this phasic activity was lost after transecting between DTAM and n.IX–X. Thus we conclude that although DTAM participates in generating vocal rhythms, it does so in coordination with neurons in n.IX–X.

LFP recordings in DTAM also identified neural correlates of vocal pattern. This slow baseline LFP wave in DTAM coincides with fictive fast and slow trills. Wave duration predicts fictive fast trill (but not introductory phase) duration and wave interval predicts slow trill duration. This tight correlation may be a simple reflection of rhythm generator activity in DTAM. However, we found that the slow wave continued after abolishing the trill-related rhythmic activity by disrupting connections with n.IX–X. Thus unlike rhythm generator activity in DTAM that requires inputs from n.IX–X, the pattern generator

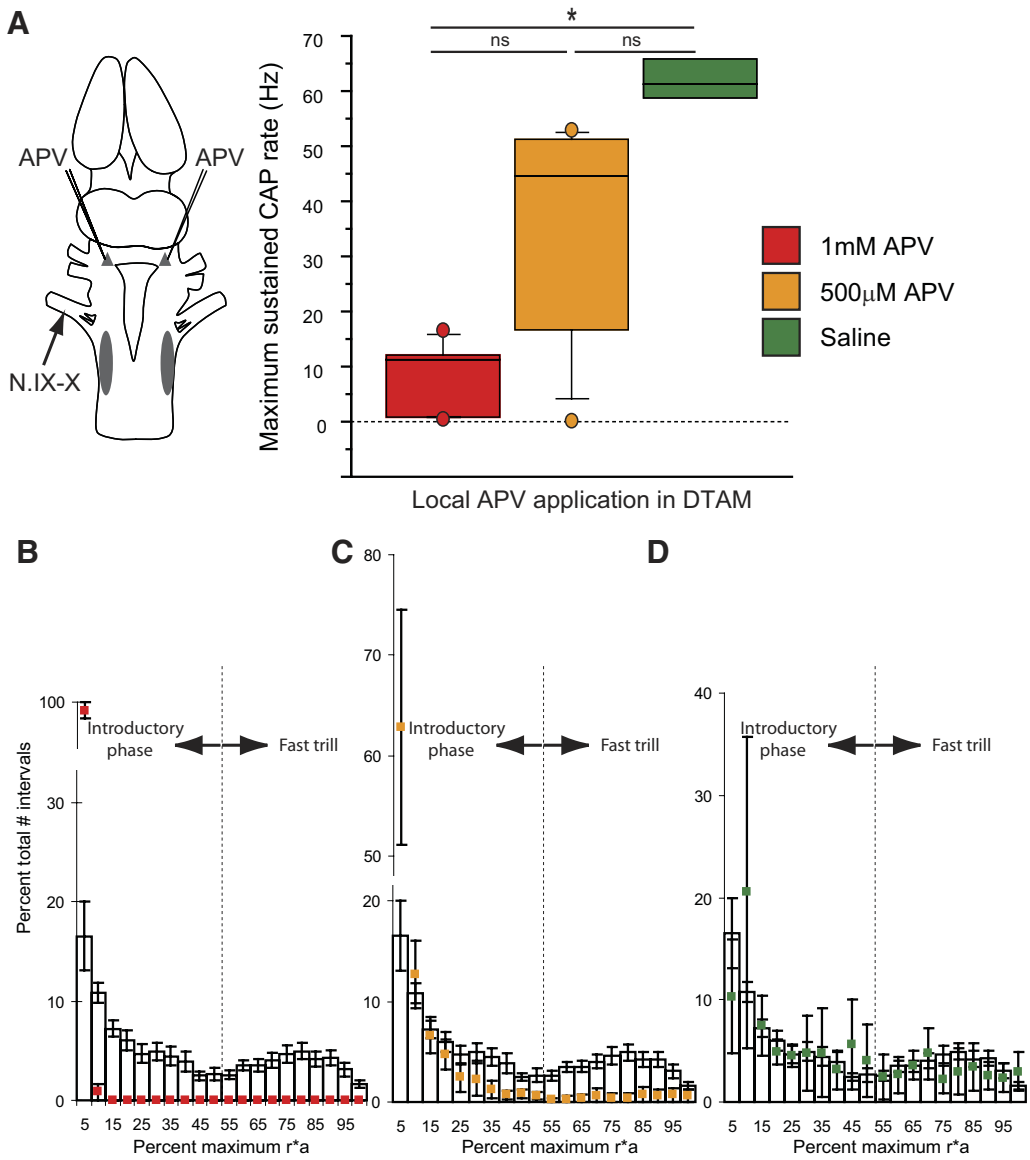

FIG. 8. Local injection of APV into DTAM blocks fictive fast trills. *A*, *left*: diagram of a brain indicating bilateral injection of APV made into DTAM; fictive vocal data were obtained by recording N.IX–X (arrow). *Right*: box plots showing the maximum sustained CAP rates obtained in saline control (green), 500 μM APV injection (orange), and 1 mM APV injection (red). Horizontal lines indicate median, boxes reflect upper and lower quartiles, whiskers indicate 5 and 95% confidence intervals, and outliers are depicted by dots. Injection of 1 mM APV into DTAM significantly reduced the maximum sustained CAP rates well below those of normal fictive fast trills ($*P < 0.05$; Kruskal–Wallis with Dunn's multiple comparison test; red box). With injections of 500 μM APV, maximum CAP rates were reduced, although the effect was not significantly different from control. *B–D*: frequency histograms showing r*a distribution during control (open bars) 5-HT application and after DTAM injections of 1 mM APV (*B*, red squares), 500 μM APV (*C*, orange squares), and saline (*D*, green squares).

is endogenous to DTAM. Taken together, we conclude that the rhythm generator and pattern generator in the vocal CPG are functionally distinct, although overlapping anatomically.

Functional homology between DTAM pattern generation and other systems

Robust anatomical connections (Zornik and Kelley 2007) and strong physiological inputs (Zornik and Kelley 2008) from DTAM to vocal and respiratory motor neurons support a potentially homologous relation between DTAM and the mammalian parabrachial nucleus (PB). The PB is an important regulator of respiratory phase in mammals (Mörschel and Dutschmann 2009; von Euler and Trippenbach 1976) and coordinates respiration with behaviors such as locomotion (Potts et al. 2005) and vocalization (Jürgens 2002). In bats, Smotherman et al. (2006) found that modulating PB activity altered call duration by changing the duration of expirations.

Similarly, amphibian DTAM may coordinate respiratory and vocal pathways. In the leopard frog, *Rana pipiens*, for example, Schmidt (1992) demonstrated that connections between DTAM and n.IX–X were required to produce fictive vocalizations and identified a "slow wave" activity that remained in DTAM after removing n.IX–X. Schmidt suggested that these "slow waves" were correlates of the expiratory phase of respiration. Because calling in *R. pipiens* is gated by expiration, the slow wave control of expiration could regulate call duration.

Although *X. laevis* evolved to produce calls dissociated from respiratory movements, the endogenous DTAM wave that we discovered here suggests that a homologous circuit and vocal gating function remains. An NMDAR-dependent circuit in *Xenopus* DTAM is consistent with NMDAR expression in rat PB (Monaghan and Cotman 1985). Thus we propose that amphibian DTAM is homologous to mammalian PB. In contrast to mammals and terrestrial frogs, the acquisition of an aquatic lifestyle by *Xenopus* has removed the need to coordinate respiratory and vocal systems, although the function of DTAM LFP waves—regulating call duration—may have been conserved through evolution.

Behavioral considerations of vocal patterning in X. laevis

Male *Xenopus* modify advertisement calls when they hear sexually receptive females calling (Tobias et al. 1998). This vocalization—the answer call—contains longer fast trills and shorter slow trills. It is possible that neuromodulator release in DTAM modifies intrinsic and synaptic properties of DTAM neurons, resulting in longer LFP waves with decreased intervals. Future determination of the cellular and synaptic mechanisms underlying DTAM waves will allow us to test for a causal relation between the DTAM wave and fast trill durations and provide the rare occasion to identify the neural basis of a motivation-dependent behavioral change.

Temperature dependence of the DTAM wave and call durations

Vocal rhythm generation in *Xenopus* is temperature dependent (Yamaguchi et al. 2008). Here, we determined that the slow LFP wave in DTAM is thermally sensitive, indicating that the rate of neuronal processing within DTAM dictates the temporal profile of the LFP wave. Because onset and offset of DTAM waves correlated tightly with fast trills, we predicted that the waves might control fast trill duration. To test this prediction, we took advantage of the temperature dependence of the wave duration by recording in vivo and fictive vocalizations at multiple temperatures. Trill and call durations (except introductory phase) and call interval were all temperature sensitive in vivo and in vitro. Furthermore, DTAM remained tightly correlated with fast trills over a wide range of trill durations, supporting the hypothesis that fast trill thermal sensitivity is endowed by inputs from the temperature-dependent wave circuit.

Q_{10} values for call durations and intervals were higher than Q_{10} values obtained previously for rhythm generation, suggesting that longer CAP intervals induced by cooler temperatures alone do not explain the longer call and trill durations. This corroborates our hypothesis that two independent circuits, with distinct thermal sensitivity, may underlie rhythm and pattern generation.

We previously showed that selectively cooling DTAM is sufficient to reduce CAP rates of both fast and slow trills (Yamaguchi et al. 2008). In this study, we reproduced the effect of DTAM cooling on CAP rates using a new selective cooling method. With this new approach, we were also able to selectively cool n.IX–X. In these experiments, fictive fast trill and introductory phase (but not slow trill) rates were reduced by n.IX–X cooling. These data imply that both n.IX–X and DTAM are capable of controlling vocal rhythm (CAP rate). However, only DTAM cooling has a significant effect on fictive call durations. Vocal pattern generation thus appears to be endogenous to DTAM. These results support the existence of distinct, but overlapping, rhythm and pattern generators.

Selective DTAM cooling elongated fictive fast trills and call intervals, but it did not affect fictive slow trill duration. One possible explanation of the results may be that DTAM waves prevent slow trills, whereas wave intervals are permissive for slow trills. Our current data support this idea; fictive slow trills occur only between waves and a strong correlation exists between fictive slow trill duration and wave intervals. In this scenario, a slow trill pattern-forming element may lie outside DTAM (possibly in n.IX–X). Thus longer intervals between waves would allow, but not guarantee, longer slow trills. For example, when DTAM was selectively cooled, fictive slow trill duration may not have changed because n.IX–X remained at room temperature. When n.IX–X was cooled, in contrast, fictive slow trills may not have been elongated because the intervals between the DTAM waves remained short, thus overriding the n.IX–X pattern generator and limiting the time available for fictive slow trills. Fictive slow trill duration was changed only during whole brain cooling, possibly because the DTAM wave intervals were elongated and the n.IX–X pattern generator was decelerated. Future LFP recordings in n.IX–X and additional temperature experiments may reveal whether vocal patterning circuits for slow trill are indeed segregated.

Surprisingly, the DTAM wave was more sensitive to temperature changes in the transected brain ($Q_{10} = 2.5 \pm 0.6$) than in the intact fictively vocalizing brain ($Q_{10} = 1.7 \pm 0.5$). Although the wave persists in isolated DTAM and selective cooling of n.IX–X did not have an obvious effect on fictive call or trill durations, the Q_{10} result raises the possibility that inputs from n.IX–X may modulate, or constrain, the DTAM wave circuit and influence vocal patterning in a minor way that was not discernible with our current techniques.

NMDARs and temporal patterning

We showed that the DTAM LFP wave is NMDAR dependent and necessary for the transition from fictive introductory phase to fast trill. NMDAR involvement in rhythmic motor programs is demonstrated in many systems. For example, fictive locomotion is induced in lamprey (Grillner et al. 1981) with NMDA application, and in rats (Cowley and Schmidt 1994), a combination of NMDA and other neuromodulators can elicit fictive locomotion. In addition, NMDARs are known to mediate the timing of motor patterns and transitions. For example, NMDARs regulate the inspiratory-to-expiratory switch in cats (Foutz et al. 1989), intersegmental delay of locomotion in frog embryos (Tunstall and Roberts 1991), expulsive phase of cough reflex in cats (Haji et al. 2008), and nitric oxide–mediated respiratory phase transition in rats (Pierrefiche et al. 2007). Thus NMDARs can control the timing of the transition from one motor stage to the next.

Changes in *Xenopus* vocal rhythms appear to be mediated by NMDAR activation in the DTAM pattern generator circuit. Because of the gradual shift from introductory phase to fast trill, a likely possibility is that a single rhythm generator circuit produces both trill rates. During the introductory phase, rhythm generator neurons may activate NMDAR-containing cells in the pattern generator. This activation might bring about the

slow wave, possibly via membrane potential oscillations or synchronous postsynaptic potentials. The wave, in turn, could initiate the transition from introductory phase to fast trill, possibly via feedback excitation onto the rhythm generator. With the offset of the wave, this excitation would cease, allowing the production of slow trill. Although the interval between DTAM waves appears to limit slow trill duration, it may not be sufficient to set slow trill durations. Thus another pattern generator component may exist elsewhere within the CPG and act in concert with the DTAM wave in controlling slow trill durations.

How might NMDAR activation regulate the LFP wave in DTAM? Excitatory postsynaptic currents induced by NMDARs are known to have a slow rise time and prolonged effect over 500 ms (Collingridge et al. 1988; Smith et al. 2000). In addition, activation of NMDARs endows neurons with bistable membrane properties, inducing membrane potential oscillations and plateau potentials (Di Prisco et al. 1997; Hochman et al. 1994; Prime et al. 1999; Tresch and Kiehn 2000; Wallen and Grillner 1987). These properties are ideal for generating long timescale activity such as the slow DTAM wave.

Regardless of the precise mechanism by which NMDARs control vocal patterning, their involvement in *Xenopus* provides an ideal system in which to study the cellular and synaptic mechanisms underlying temporal organization of pattern generation. These investigations will outline the broader capabilities of this channel, perhaps shedding new understanding on other more complicated NMDAR-dependent networks.

ACKNOWLEDGMENTS

We thank T. Gardner, D. Kelley, M. Wachowiak, and three anonymous reviewers for helpful comments on this manuscript and A. Herrold and W. Pong for collecting vocal data.

Present address of H. Rhodes: Dennison University, Department of Biology, 350 Ridge Road, Granville, OH 43023.

GRANTS

This work was supported by National Institute of Neurological Disorders and Stroke Grant R01 NS-048834, start-up funds provided by Boston University, and a Claire Boothe Luce Professorship to A. Yamaguchi.

DISCLOSURES

No conflicts of interest are declared by the authors.

REFERENCES

Brahic CJ, Kelley DB. Vocal circuitry in *Xenopus laevis*: telencephalon to laryngeal motor neurons. *J Comp Neurol* 464: 115–130, 2003.

Collingridge GL, Herron CE, Lester RA. Frequency-dependent *N*-methyl-D-aspartate receptor-mediated synaptic transmission in rat hippocampus. *J Physiol* 399: 301–312, 1988.

Cowley KC, Schmidt BJ. A comparison of motor patterns induced by *N*-methyl-D-aspartate, acetylcholine and serotonin in the in vitro neonatal rat spinal cord. *Neurosci Lett* 171: 147–150, 1994.

Daw NW, Stein PS, Fox K. The role of NMDA receptors in information processing. *Annu Rev Neurosci* 16: 207–222, 1993.

Di Prisco GV, Pearlstein E, Robitaille R, Dubuc R. Role of sensory-evoked NMDA plateau potentials in the initiation of locomotion. *Science* 278: 1122–1125, 1997.

Foutz AS, Champagnat J, Denavit-Saubie M. Involvement of *N*-methyl-D-aspartate (NMDA) receptors in respiratory rhythmogenesis. *Brain Res* 500: 199–208, 1989.

Grillner S, McClellan A, Sigvardt K, Wallen P, Wilen M. Activation of NMDA-receptors elicits "fictive locomotion" in lamprey spinal cord in vitro. *Acta Physiol Scand* 113: 549–551, 1981.

Haji A, Ohi Y, Tsunekawa S. *N*-Methyl-D-aspartate mechanisms in depolarization of augmenting expiratory neurons during the expulsive phase of fictive cough in decerebrate cats. *Neuropharmacology* 54: 1120–1127, 2008.

Hochman S, Jordan LM, MacDonald JF. *N*-Methyl-D-aspartate receptor-mediated voltage oscillations in neurons surrounding the central canal in slices of rat spinal cord. *J Neurophysiol* 72: 565–577, 1994.

Janssen R. Thermal influences on nervous system function. *Neurosci Biobehav Rev* 16: 399–413, 1992.

Jürgens U. Neural pathways underlying vocal control. *Neurosci Biobehav Rev* 26: 235–258, 2002.

Kelley DB. Auditory and vocal nuclei in the frog brain concentrate sex hormones. *Science* 207: 553–555, 1980.

Monaghan DT, Cotman CW. Distribution of *N*-methyl-D-aspartate-sensitive L-[3H]glutamate-binding sites in rat brain. *J Neurosci* 5: 2909–2919, 1985.

Mörschel M, Dutschmann M. Pontine respiratory activity involved in inspiratory/expiratory phase transition. *Philos Trans R Soc Lond B Biol Sci* 364: 2517–2526, 2009.

Pierrefiche O, Abdala AP, Paton JF. Nitric oxide and respiratory rhythm in mammals: a new modulator of phase transition? *Biochem Soc Trans* 35: 1258–1263, 2007.

Potts JT, Rybak IA, Paton JF. Respiratory rhythm entrainment by somatic afferent stimulation. *J Neurosci* 25: 1965–1978, 2005.

Prime L, Pichon Y, Moore LE. *N*-Methyl-D-aspartate-induced oscillations in whole cell clamped neurons from the isolated spinal cord of *Xenopus laevis* embryos. *J Neurophysiol* 82: 1069–1073, 1999.

Rhodes HJ, Yu HJ, Yamaguchi A. Xenopus vocalizations are controlled by a sexually differentiated hindbrain central pattern generator. *J Neurosci* 27: 1485–1497, 2007.

Schmidt RS. Neural correlates of frog calling: production by two semi-independent generators. *Behav Brain Res* 50: 17–30, 1992.

Simpson HB, Tobias ML, Kelley DB. Origin and identification of fibers in the cranial nerve IX–X complex of *Xenopus laevis*: Lucifer Yellow backfills *in vitro*. *J Comp Neurol* 244: 430–444, 1986.

Smith AJ, Owens S, Forsythe ID. Characterisation of inhibitory and excitatory postsynaptic currents of the rat medial superior olive. *J Physiol* 529: 681–698, 2000.

Smotherman M, Kobayasi K, Ma J, Zhang S, Metzner W. A mechanism for vocal-respiratory coupling in the mammalian parabrachial nucleus. *J Neurosci* 26: 4860–4869, 2006.

Tobias ML, Barnard C, O'Hagan R, Horng S, Rand M, Kelley DB. Vocal communication between male *Xenopus laevis*. *Anim Behav* 67: 353–365, 2004.

Tobias ML, Viswanathan SS, Kelley DB. Rapping, a female receptive call, initiates male-female duets in the South African clawed frog. *Proc Natl Acad Sci USA* 95: 1870–1875, 1998.

Tresch MC, Kiehn O. Motor coordination without action potentials in the mammalian spinal cord. *Nat Neurosci* 3: 593–599, 2000.

Tunstall MJ, Roberts A. Longitudinal coordination of motor output during swimming in Xenopus embryos. *Proc Biol Sci* 244: 27–32, 1991.

von Euler C, Trippenbach T. Excitability changes of the inspiratory "off-switch" mechanism tested by electrical stimulation in nucleus parabrachialis in the cat. *Acta Physiol Scand* 97: 175–188, 1976.

Wallen P, Grillner S. *N*-Methyl-D-aspartate receptor-induced, inherent oscillatory activity in neurons active during fictive locomotion in the lamprey. *J Neurosci* 7: 2745–2755, 1987.

Wetzel DM, Haerter UL, Kelley DB. A proposed neural pathway for vocalization in South African clawed frogs, *Xenopus laevis*. *J Comp Physiol A Sens Neural Behav Physiol* 157: 749–761, 1985.

Wetzel DM, Kelley DB. Androgen and gonadotropin effects on male mate calls in South African clawed frogs, *Xenopus laevis*. *Horm Behav* 17: 388–404, 1983.

Yamaguchi A, Gooler D, Herrold A, Patel S, Pong WW. Temperature-dependent regulation of vocal pattern generator. *J Neurophysiol* 100: 3134–3143, 2008.

Yu HJ, Yamaguchi A. Endogenous serotonin acts on 5-HT2C-like receptors in key vocal areas of the brain stem to initiate vocalizations in *Xenopus laevis*. *J Neurophysiol* 103: 648–658, 2010.

Zornik E, Kelley DB. Breathing and calling: neuronal networks in the *Xenopus laevis* hindbrain. *J Comp Neurol* 501: 303–315, 2007.

Zornik E, Kelley DB. Regulation of respiratory and vocal motor pools in the isolated brain of Xenopus laevis. *J Neurosci* 28: 612–621, 2008.